A Wireless Fully-Passive Neural Recording Device for Unobtrusive Neuropotential Monitoring

Asimina Kiourti, *Member, IEEE*, Cedric W. L. Lee, *Student Member, IEEE*, Junseok Chae, *Senior Member, IEEE*, and John L. Volakis, *Fellow, IEEE*,

***Abstract*— *Goal*: We propose a novel wireless, fully-passive neural recording device for unobtrusive neuropotential monitoring. Previous work demonstrated the feasibility of monitoring emulated brain signals in a wireless fully-passive manner. In this paper, we propose a novel, realistic recorder that is significantly smaller and much more sensitive. *Methods*: The proposed recorder utilizes a highly-efficient microwave backscattering method and operates without any formal power supply or regulating elements. Also, no intra-cranial wires or cables are required. *In-vitro* testing is performed inside a 4-layer head phantom (skin, bone, grey matter, and white matter). *Results*: Compared to our former implementation, the neural recorder proposed in this work has the following improved features: (a) 59% smaller footprint, (b) up to 20 dB improvement in neuropotential detection sensitivity, and (c) encapsulation in biocompatible polymer. *Conclusion*: For the first time, temporal emulated neuropotentials as low as 63 μV_{pp} can be detected in a wireless fully-passive manner. Remarkably, the high-sensitivity achieved in this work implies reading of most neural signals generated by the human brain. *Significance*: The proposed recorder brings forward transformational possibilities in wireless fully-passive neural detection for a very wide range of applications (e.g., epilepsy, Alzheimer's, mental disorders, etc.).**

***Index Terms*—Anti-parallel diode pair, biocompatibility, biomedical telemetry, brain implant, miniaturization, neurosensing, passive circuits, sub-harmonic mixer.**

I. Introduction

BRAIN implant technology has a strong potential to improve the individual's well-being. Example applications include: early detection of epileptic seizures, treatments and prosthetics for the disabled, understanding and improving the brain's functionality for people with Alzheimer's, mental disorders, addictions, etc. [1]-[5]. However, current/in-research brain implants lack the safety and reliability required for unobtrusive, long-term monitoring of neuropotentials.

Specifically, in several cases, wires have been used to connect intra-cranial clinical implants to the exterior monitoring units [3], [6]. As would be expected, recording of neural data under tethered connections is restricted to clinical studies in static environments. This limits the range of possible brain science research and applications. Recently, the aforementioned limitation has been overcome using wireless brain implants. Nevertheless, a number of safety-related issues still exist. For example, the work in [7], [8] considered wireless neural tags for RFID-inspired brain-machine interfaces. Though batteries were avoided, RF-to-DC converters and power storage devices were still used, implying heat generation issues. This heating might disturb normal brain operation and eventually damage the cerebral tissue [9] [10]. In another case [11], a wireless neurosensor was presented for recording electrophysiological signals from the cortex of monkeys. However, the latter neurosensor employed a head-mounted device with a "screw-on" interconnect to the implant. That is, the skull was always perforated by wires, limiting natural lifestyle and comfort, if such system pursues for human subjects.

As an alternative, we aim to establish a novel technology for carefree, safe and reliable brain implants. Our objectives entail: (a) fully-passive implants (no battery, energy harvesting unit, or rectifier/regulator), (b) wireless operation for unobtrusive monitoring with minimum impact to the individual's activity, (c) extremely simple electronics that generate minimal heat, and (d) tiny footprint to minimize trauma [12], [13]. Recently, we demonstrated a proof-of-concept wireless fully-passive neural recording device with high detection sensitivity [13]. Specifically, in frequency-domain, the implant in [13] could detect emulated brain signals of 200 μV_{pp} at f_{neuro} = 100 Hz, to as low as 50 μV_{pp} at f_{neuro} = 1 kHz. In time-domain, the aforementioned device could detect neuropotentials of 670 μV_{pp} at f_{neuro} = 100 Hz, to as low as 200 μV_{pp} at f_{neuro} = 1 kHz. However, to be able to read all neural signals generated by the human brain (see Table I [1], [14]-[16]), further improvement in sensitivity is needed. We also remark that the proof-of-concept implant

Manuscript received February 11, 2015, revised May 04, 2015, accepted July 16, 2015. This material is based upon work supported by the National Science Foundation under Grant No. 1344825.

A. Kiourti, C. W. L. Lee, and J. L. Volakis are with the ElectroScience Laboratory, Department of Electrical & Computer Engineering, The Ohio State University, Columbus, OH 43212 USA (e-mail: kiourti.1@osu.edu; lee.6256@osu.edu; volakis.1@osu.edu).

J. Chae is with the School of Electrical, Computer, and Energy Engineering, Arizona State University, Tempe, AZ 85287 USA (e-mail: Junseok.Chae@asu.edu).

TABLE I
VOLTAGE AND FREQUENCY RANGE OF SIGNALS GENERATED BY THE HUMAN BRAIN

Neural signals	Voltage Range	Frequency Range (f_{neuro})
ElectroCorticographic (ECoG) signals	100 – 200 μV_{pp}	< 500 Hz
Neural "spikes"	100 – 2000 μV_{pp}	300 Hz – 5 kHz
Local Field Potentials (LFPs)	20 – 2000 μV_{pp}	< 500 Hz

reported in [13] was big (footprint of 39 mm × 15 mm) and non-biocompatible. Thus, it was unsuitable for realistic applications.

In this paper, we build upon our previous work [13] to design a novel wireless fully-passive neural recording device that: (a) has 59% smaller footprint, (b) exhibits up to 20 dB improvement in neuropotential detection sensitivity, and (c) is encapsulated in biocompatible polymer. To mimic realistic implantation scenarios, the device is tested inside a 4-layer (skin, bone, grey matter, white matter) head phantom [17]-[19]. For the first time, temporal emulated neuropotentials as low as 63 μV_{pp} can be detected. Thus, most neural signals generated by the human brain (see Table I) can now be recorded in a fully-passive and wireless manner. In doing so, the neural recorder brings forward transformational possibilities for a very wide range of applications.

II. NEUROSENSING SYSTEM OVERVIEW

The block diagram of our neurosensing system is summarized in Fig. 1. It consists of: (1) the implanted sensor to be placed just above the grey matter of the human brain, and (2) the exterior interrogator, placed right outside the scalp and can be incorporated within a cap or a textile band [20]. Compared to [13], the neural recording device employed in this work is significantly smaller and biocompatible, and has much higher detection sensitivity (viz. 10x better). Also, the neurosensing system now integrates a synchronous RF demodulator. The latter is used to downconvert the detected neuropotentials to baseband, and display the retrieved temporal waveforms on an oscilloscope.

The wireless and fully-passive acquisition of neural signals deploys the microwave backscattering effect [12]. In brief, on-board non-linear components, viz. diodes, mix an externally supplied high-frequency microwave carrier with the low-frequency neural signals. The mixing products are then backscattered to the external reader where the original neural signals are retrieved. Fig. 1 illustrates the neurosensing system block diagram. The exterior interrogator sends a carrier (2.4 GHz) to activate the recorder. That, in return, detects brain signals (f_{neuro}) via a pair of wires/electrodes, and mixes them with the carrier to generate 3rd order mixing products at 4.8 GHz ± f_{neuro}. The latter are then transmitted back to the interrogator. Harmonic mixing at twice the carrier frequency is selected so as to enhance isolation between the transmit (2.4 GHz) and receive (4.8 GHz ± f_{neuro}) signals. For wireless transmission, a pair of highly-coupled antennas are employed,

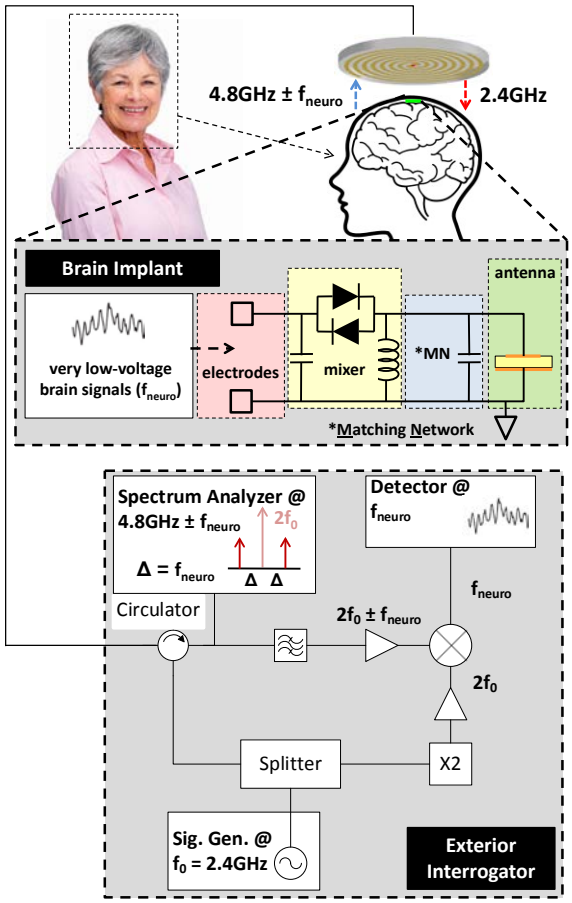

Fig. 1. Neurosensing system block diagram.

viz. a 0.6 - 6 GHz interrogator spiral [13], [21], and a dual-band (2.4 / 4.8 GHz) implanted patch.

At the interrogator, the backscattered signals (4.8 GHz ± f_{neuro}) can be viewed through a spectrum analyzer (frequency-domain), or demodulated and displayed on an oscilloscope (time-domain). In this study, an RF synchronous demodulator was employed [22], [23]. A simplified version of this demodulator is shown in Fig. 1. In brief, the demodulator mixes the received signals (4.8 GHz ± f_{neuro}) with a reference 4.8 GHz to retrieve the baseband neuropotentials (f_{neuro}). To improve the final signal-to-noise ratio, multiple stages of filtering and amplification were used [23].

III. BRAIN IMPLANT DESIGN

The neural recorder consists of: 1) the miniaturized dual-band (2.4 / 4.8 GHz) antenna that receives the carrier signal at 2.4 GHz and backscatters the 3rd order mixing products at 4.8 GHz ± f_{neuro}, and 2) the circuit that mixes the neural signals (f_{neuro}) with the carrier to backscatter 4.8 GHz ± f_{neuro}. Mixing is performed via a high-efficiency sub-harmonic mixer employing an anti-parallel diode pair (APDP). This is a unique aspect of our design and was analyzed in [13]. In this work, we further improve the mixing efficiency, by employing a capacitor and an inductor in parallel to the APDP mixer (see Fig. 1) [24]: the capacitor (100 pF) provided the path to ground for the high-frequency carrier (2.4 GHz), whereas the

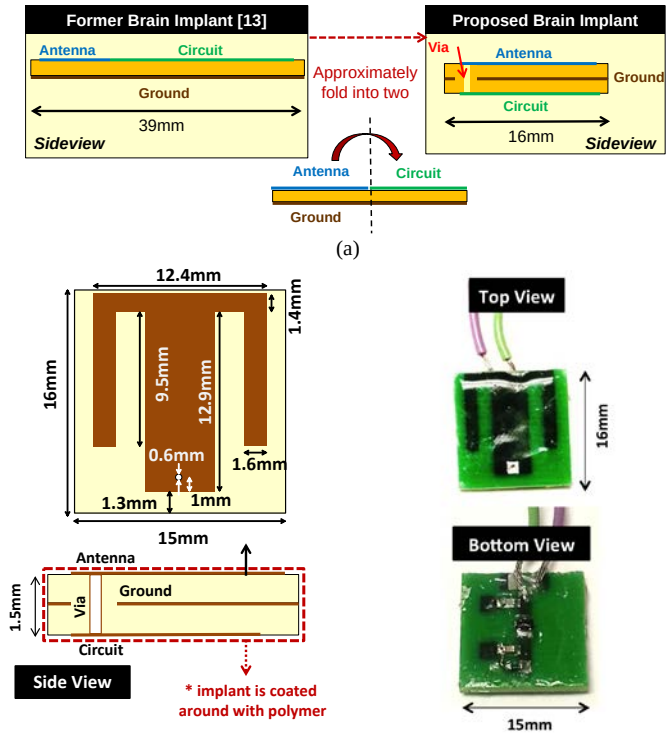

Fig. 2. Proposed brain implant: (a) idea for miniaturization, (b) implanted antenna, and (c) fabricated prototype.

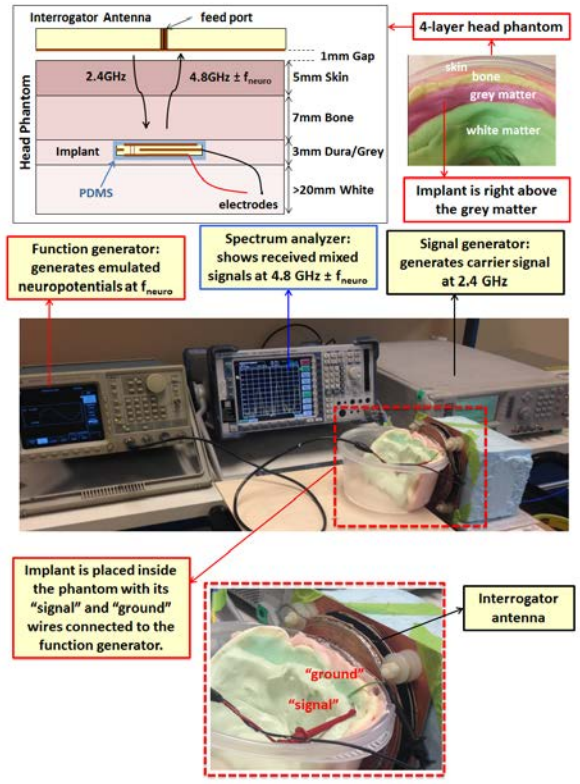

Fig. 3. Measurement set-up with 4-layer head phantom.

inductor (6.8 μH) provided the path to ground for the low-frequency neuropotentials (f_{neuro}). A matching capacitor (0.1 pF) was also used to match the impedance of the miniaturized antenna to that of the mixer.

Fig. 2 shows the recorder design. It has a footprint of 16 mm x 15 mm, viz. 59% smaller than our former implementation [13]. As shown in Fig. 2(a), the key idea for miniaturization was to "fold" our former implant [13] approximately into two, and re-design accordingly. Specifically, the device in [13] employed a single substrate layer, or, equivalently, two metallization layers. The on-board circuit and antenna were printed on the top metallization layer, while the ground plane was printed on the bottom metallization layer. Instead, the neural recorder in this work employs two substrate layers (of 59% smaller footprint than [13]), or, equivalently, three metallization layers. The on-board circuit, antenna, and ground plane were printed on the bottom, top, and middle metallization layer, respectively. A plated *via* was then used to connect the circuit and antenna to ground. The employed dual-band (2.4 / 4.8 GHz) on-board antenna was a modified version of the one presented in [13]. Its design is shown in Fig. 2(b).

To ensure biocompatibility, the recorder was coated with a thin layer of polydimethylsiloxane (PDMS) polymer (ε_r = 2.8, tanδ = 0.001). We remark that PDMS has very similar electrical properties to Silastic® MDX4-4210 Biomedical Grade Elastomer [25], which has long been used in medical implants. Concurrently, this coating acts as a low-loss superstrate to the antenna, reducing power absorbed by the human body, and increasing the transmission coefficient between the on-board and interrogator antennas [26] [27]. This implies reduction of the overall system loss, and thus, improvement of the system's neuropotential detection sensitivity.

As would be expected, in designing the circuit and antenna, we took into account the effect of (a) both substrate layers, (b) surrounding polymer coating, and (c) plated *via*. The mixer circuit was optimized for low conversion loss using Harmonic Balance analysis in Agilent® Advanced Design System (ADS). The implanted antenna was optimized in ANSYS® HFSS to achieve high transmission coefficient ($|S_{21}|$) at 2.4 GHz and 4.8 GHz in presence of the exterior interrogator spiral [13]. Finally, the matching capacitor (see Fig. 1) was optimized in ADS to minimize mismatch losses between the on-board antenna and mixer circuit. The fabricated prototype is shown in Fig. 2(c). FR-4 substrate (ε_r = 4.6, tanδ = 0.016) layers were used, each with a thickness of 31 mils (0.789 mm). To ensure biocompatibility, a bubble-free PDMS mixture was carefully poured onto the implant. A curing process was then conducted under elevated temperature (~100°C).

Table II highlights the unique features of the proposed recorder vs. previously reported wireless devices. To our knowledge, [12] and [13] are the only wireless fully–passive neural recorders reported to date. However, the recorder in [12] could not read most of the signals generated by the human brain (see Table I). The recorder in [13] had much higher sensitivity, but it was bulky and not biocompatible. In this paper, we build upon the operating principles reported in

TABLE II
COMPARISON OF PROPOSED VS. PREVIOUSLY REPORTED WIRELESS IMPLANTED NEURAL RECORDING DEVICES

Ref.	Type	Footprint	Power consumption	Transmission technology	Operation distance	Min. detectable signal
[11]	Exterior	52 x 44 mm^2	17 mA from a 1.2 Ah battery to run for 48 hours	3.1 - 5 GHz OOK	< 5 m	N/A
[28]	Exterior	N/A	645 mW	2.38 GHz FM	< 60 m	10.2 μV_{pp} (rat)
[29]	Exterior	50 x 40 mm^2	100 mW	916.5 MHz ASK	2 m	N/A
[30]	Exterior	38 x 38 mm^2	142 mW	3.9 GHz FSK	< 20 m	14.2 μV_{pp} (non-human primate)
[31]	Exterior	N/A	5.6 mW	898/926 MHz FSK	1 m	13.9 μV_{pp} (rat)
[32]	Exterior	14 x 16 mm^2	14.4 mW	70/200 MHz OOK	1 cm	25.2 μV_{pp} (guinea)
[33]	Implanted	56 x 42 mm^2	90.6 mW	3.2/3.8 GHz FSK	1-3 m	24.3 μV_{pp} (non-human primate)
[34]	Implanted	50 x 40 mm^2	2000 mW	916.5 MHz ASK	< 2.2 m	20 μV_{pp} (sheep)
[35]	Implanted	14 x 15.5 mm^2	14.4 mW	70-200 MHz FSK	N/A	23 μV_{pp} (guinea)
[7]-[8]	Implanted	N/A	N/A, yet >0 mW	N/A	2 cm	N/A
[12] [36]	Implanted	12 x 4 mm^2	0 mW	Fully-passive backscattering	< 1.5 cm	6000 μV_{pp} (in-vitro) 500 μV_{pp} (frog)
[13]	Implanted	39 x 15 mm^2	0 mW	Fully-passive backscattering	8 mm	200 μV_{pp} (in-vitro)
Proposed	Implanted	16 x 15 mm^2	0 mW	Fully-passive backscattering	~ 1.5 cm (on-body portable receiver envisioned)	63 μV_{pp} (in-vitro)

N/A: non-available

TABLE III
PHANTOM FORMULAS

Ingredients	Skin	Bone	Grey Matter	White Matter
Deionized Water	65.4%	49.3%	75.2%	59.6%
NaCl	0.1%	0.001%	0.1%	0.1%
Agar	3.9%	4.9%	4.5%	5.6%
Boric Acid	1.2%	1.5%	1.4%	1.0%
TX-151	3.2%	4.9%	3.8%	3.9%
Polyethylene Powder	26.2%	39.4%	15%	29.8%

[13] to develop a novel, realistic, recorder that can read almost all signals generated by the human brain (see Table I), and has much smaller footprint, 16×15mm^2. We remark that the large sensitivity improvement of the proposed design is attributed to: (a) new implanted antenna that exhibits much higher coupling with the exterior interrogating antenna, (b) improved matching between the implanted circuit and antenna, and (c) improved performance of the implanted mixer. The latter was mainly due to the inclusion of the 6.8 μH inductor that provided a path to ground for the low-frequency neuropotentials (f_{neuro}).

IV. SYSTEM PERFORMANCE

A. Measurement Set-Up

The measurement set-up used to assess the sensitivity (i.e., the minimum detectable emulated neuropotentials) of the neurosensing system is shown in Fig. 3. The 2.4 GHz carrier was generated by a signal generator (transmit power of 16 dBm) and fed to the interrogator spiral antenna via a circulator. Emulated neuropotentials at f_{neuro} = 100 Hz – 5 kHz were generated through an arbitrary waveform generator. The recorder was immersed inside a 4-layer head phantom that emulated skin, bone, grey matter, and white matter tissues. We remark that, for the ease of experimental testing, the dura and grey matter layers were combined as one [18]. The latter was made possible since the dura layer: (a) is very thin (< 0.5 mm), and (b) has very similar electrical properties to grey matter [19]. Fig. 3 shows the implant's position with respect to the stacked layers, as well as the individual layer thicknesses.

Phantom formulas were adapted from [17] and are given in Table III. In brief, polyethylene powder and sodium chloride (NaCl) were used to adjust the phantom's permittivity and conductivity, respectively. Self-shaping was made possible with agar, while TX-151 was used to increase the mixture's viscosity. Boric acid was finally added as a preservative.

The permittivity and conductivity of each emulated tissue were measured using the Agilent® 85070E Dielectric Probe Kit. Measured vs. reference ("target") [19] electrical properties are shown in Fig. 4 as a function of frequency. As seen, good agreement exists throughout the entire frequency range of interest. For all layers, measured permittivity at 2.4 GHz and 4.8 GHz was within ±4.3 error from the reference values. Measured conductivity at 2.4 GHz and 4.8 GHz was within ±0.6 error from the reference values.

B. System Sensitivity

1) Frequency-Domain Performance

The received (4.8 GHz ± f_{neuro}) signals were first detected via a spectrum analyzer at the interrogator side (see Fig. 1). An example measured spectral response is shown in the inset of Fig. 5. System loss was then calculated by subtracting the received sideband power level (at 4.8 GHz ± f_{neuro}) from the generated neuropotential power (at f_{neuro}). We note that system loss (L_{sys}) may be defined as:

$$L_{sys}\,[dB] = L_{conv}\,[dB] + L_{propag}[dB] + L_{match}\,[dB] \quad (1)$$

where L_{conv} is the mixer conversion loss, L_{propag} is the propagation loss (i.e., transmission loss, $|S_{21}|$ between the on-board and interrogator antennas), and L_{match} is the matching loss between the on-board antenna and mixer circuit. This breakdown is very useful in the design phase, as minimization

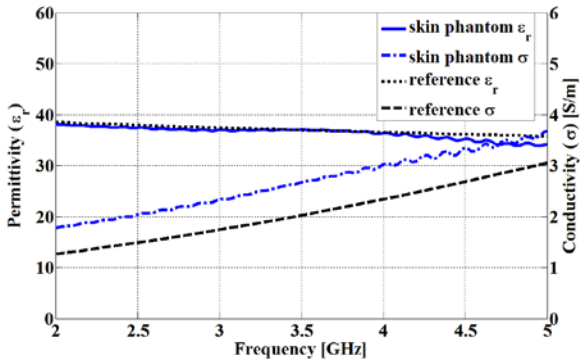

(a)

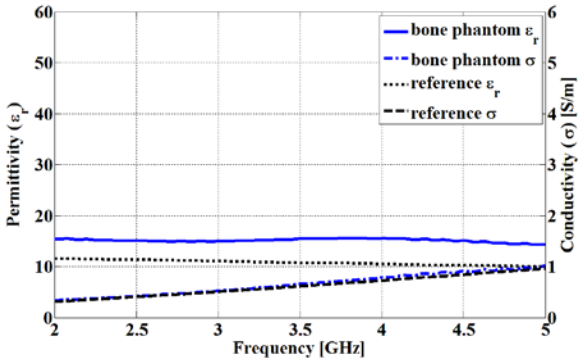

(b)

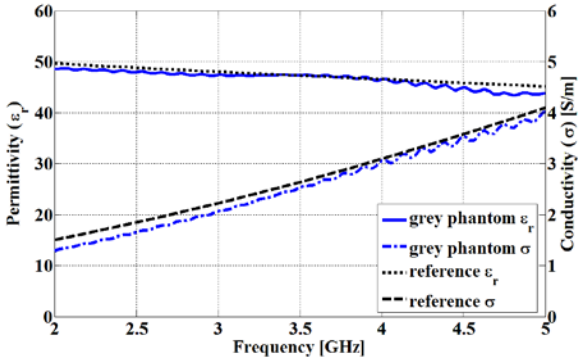

(c)

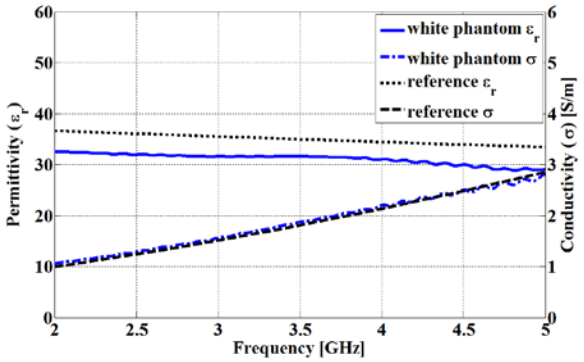

(d)

Fig. 4. Phantom electrical properties vs. reference values [19]: (a) skin, (b) bone, (c) grey matter, and (d) white matter.

of each individual loss component improves the overall system sensitivity accordingly. As shown in Fig. 5, system loss was measured to be 40 dB at f_{neuro} = 100 Hz – 5 kHz. This was only ~4 dB higher than simulations, likely due to diode

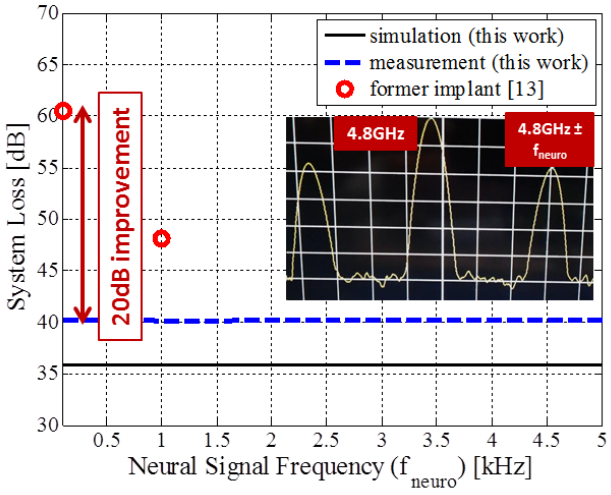

Fig. 5. System loss as a function of f_{neuro}. (inset shows an example received spectral response)

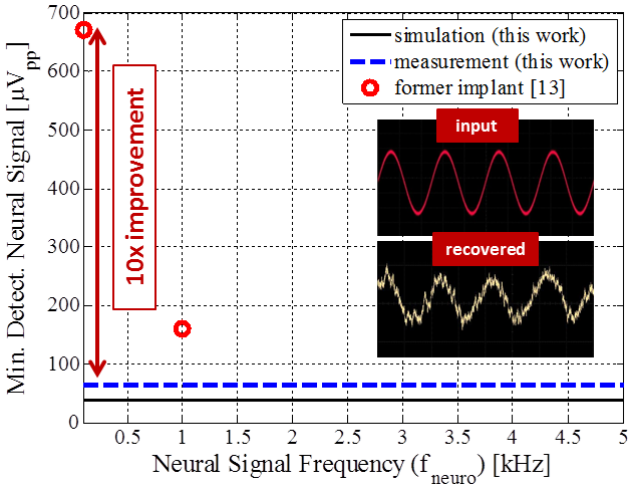

Fig. 6. Minimum detectable neuropotentials in time-domain as a function of f_{neuro}. (inset shows example input vs. recovered neuropotential waveforms)

packaging losses and discrepancies in phantom layer thicknesses. Remarkably, compared to our former implementation [13], the neurosensing system exhibits up to 20 dB lower loss. Of course, this implies an equivalent, 20 dB, improvement in system sensitivity. Assuming a minimum detectable signal of -130 dBm at the spectrum analyzer [13], frequency-domain emulated neural signals as low as 20 μV_{pp} can be detected at f_{neuro} = 100 Hz – 5 kHz. This is an up to 10x improvement in sensitivity compared to [13].

2) Time-Domain Performance

To assess the minimum detectable emulated neuropotentials of the neurosensing system in time-domain, we proceeded to downconvert the backscattered (4.8 GHz ± f_{neuro}) signals to baseband (f_{neuro}). To do so, we employed an RF synchronous demodulator at the interrogator side, see Fig. 1. The recovered emulated neuropotentials were then viewed through an oscilloscope. Fig. 6 shows the minimum detectable emulated neuropotentials in time-domain. The latter were obtained as:

$$MDS_{Neuro}\,[dBm] = MDS_{RX}\,[dBm] + L_{sys}[dB] \quad (2)$$

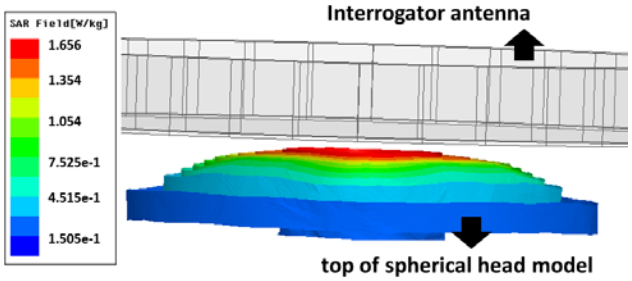

Fig. 7. 10 g-averaged SAR distribution at 2.4 GHz within a 10 cm-radius spherical head model, assuming an interrogator power of 16 dBm.

where MDS_{Rx} is the minimum detectable signal at the receiver, and L_{sys} is the system loss from (1). For the employed interrogator, MDS_{RX} was:

$$MDS_{RX}\,[dBm] = kT(dBm/Hz) + log_{10}\,5kHz + NF + SNR$$
$$= -174 + 37 + 4 + 13 = -120\,dBm \qquad (3)$$

where kT is the thermal noise power, NF is the receiver noise figure, and SNR is the receiver signal to noise ratio. As seen in Fig. 6, the neurosensing system can detect temporal emulated brain signals as low as 63 μV_{pp} at f_{neuro} = 100 Hz – 5 kHz. Compared to our previous implementation [13], this is an up to 10x improvement in sensitivity. Importantly, this high sensitivity implies reading of most signals generated by the human brain in a fully-passive and wireless manner (see Table I). Example input vs. recovered emulated neuropotential waveforms are shown in the inset of Fig. 6.

C. Specific Absorption Rate (SAR) Performance

To assess conformance of the neurosensing system to patient safety guidelines, we carried out numerical Specific Absorption Rate (SAR) studies in ANSYS® HFSS. For these studies, we considered a 10 cm-radius spherical head model [37] consisting of skin, bone, grey matter, and white matter tissues. The recorder was placed in between the dura and grey matter, while the interrogator antenna was placed right outside the scalp. The SAR distribution at 2.4 GHz averaged over 10 g of tissue is shown in Fig. 7. The latter is for a transmit interrogator power of 16 dBm. As seen, $SAR_{10g,max}$ = 1.65 W/kg. Therefore, the neurosensing system satisfies the IEEE C95.1-2005 [38] guidelines for uncontrolled environment exposure, viz. $SAR_{10g,max}$ < 2 W/kg. We also note that $SAR_{1g,max}$ = 7.38 W/kg. Therefore, at this point, the system further satisfies the FCC [39] safety guidelines for controlled environment exposure, viz. $SAR_{1g,max}$ < 8 W/kg. Future implementations will consider further reduction of the interrogator's transmit power levels.

V. Conclusion

A wireless fully-passive neurosensing system was presented for continuous and unobtrusive monitoring of very-low-voltage brain signals. This type of fully-passive and wireless neuropotential acquisition has the unique property of very minor heating, thus, minimizing injury and trauma to the brain while preserving natural lifestyle and comfort. Our previous work had demonstrated the feasibility of monitoring emulated brain signals in a wireless fully-passive manner. In this paper, we took a major step forward by proposing a novel, realistic, recorder that exhibits the following unique features: (a) 59% smaller footprint, (b) up to 20 dB improvement in sensitivity, and (c) encapsulation in biocompatible polymer. To better reflect the actual implantation scenario, *in-vitro* testing was performed inside a 4-layer (skin, bone, grey matter, white matter) head phantom.

For the first time, detection of emulated temporal neural signals as low as 63 μV_{pp} was demonstrated, viz. up to 10x lower than [13]. This high sensitivity implies that most signals generated by the human brain can be read in a fully-passive and wireless manner. In doing so, the neurosensing system brings forward novel capabilities for a very wide range of applications (e.g., epilepsy monitoring, prosthetics control, early seizure detection, trauma assessment, etc).

Future work will include further implant miniaturization and *in-vivo* testing inside animal models.

References

[1] G. Schalk and E.C. Leuthardt, "Brain–computer interfaces using electrocorticographic signals," *IEEE Rev. Biomed.* Eng., vol. 4, pp. 140–154, 2011.
[2] D.R. Kipke *et al.*, "Advanced neurotechnologies for chronic neural interfaces: new horizons and clinical opportunities," *J. Neurosc.*, vol. 28, no. 46, pp. 11830–11838, 2008.
[3] K.D. Wise, "Microelectrodes, microelectronics, and implantable neural microsystems," *Proc. IEEE*, vol. 96, no. 7, pp. 1184–1202, Jul. 2008.
[4] J.P. Blount *et al.*, "Advances in intracranial monitoring," *Neurosurg. Focus*, vol. 25, no. 3, pp. 1–8, Sept. 2008.
[5] P. Nuyujukian *et al.*, "A high-performance keyboard neural prosthesis enabled by task optimization," *IEEE Trans. Biomed. Eng.*, vol. 62, no. 1, pp. 21-29, Jan. 2015.
[6] A. Waziri *et al.*, "Initial surgical experience with a dense cortical microarray in epileptic patients undergoing craniotomy for subdural electrode implantation," *Neurosurg.*, vol. 64m pp. 540–545, 2009.
[7] E. Moradi *et al.*, "Measurement of wireless link for brain–machine interface systems using human–head equivalent liquid," *IEEE Antennas Wireless Propag. Lett.*, vol. 12, pp. 1307–1310, 2013.
[8] E. Moradi *et al.*, "Miniature implantable and wearable on–body antennas: towards the new era of wireless body–centric systems," *IEEE Antennas Propag. Mag.*, vol. 56, no. 1, pp. 271–291, Feb. 2014.
[9] S. Kim *et al.*, "Thermal impact of an active 3-D microelectrode array implanted in the brain," *IEEE Trans. Neural Syst. Rehab. Eng.*, vol. 15, pp. 493–501, 2007.
[10] Q. Tang *et al.*, "Communication scheduling to minimize thermal effects of implanted biosensor networks in homogeneous tissue," *IEEE Trans. Biomed. Eng.*, vol. 52, pp. 1285–1294, 2005.
[11] M. Yin *et al.*, "Wireless neurosensor for full-spectrum electrophysiology recordings during free behavior," *Neuron.*, vol. 84, pp. 1-13, 2014.
[12] H.N. Schwerdt *et al.*, "A fully passive wireless microsystem for recording of neuropotentials using RF backscattering methods," *J. Microelectromech. Syst.*, vol. 20, pp. 1119–1130, Oct. 2011.
[13] C.W.L. Lee *et al.*, "A high-sensitivity fully-passive neurosensing system for wireless brain signal monitoring," *IEEE Trans. Microw. Theory Techn.*, vol. 63, pp. 2060–2068, Jun. 2015.
[14] R.R. Harrison, "Design of integrated circuits to observe brain activity," *Proc. IEEE*, vol. 96, no. 7, pp. 1203-1216, Jul. 2008.
[15] R.R. Harrison, "A versatile integrated circuit for the acquisition of biopotentials," in *Proc. IEEE Custom. Integr. Circ. Conf.*, pp. 115-122, 2007.
[16] S.P. Burns *et al.*, "Comparisons of the dynamics of local field potential and multi-unit activity signals in macaque visual cortex," *J. Neurosc.*, vol. 30, no. 41, pp. 13739-13749, Oct. 2010.
[17] K. Ito *et al.*, "Development and characteristics of a biological tissue-equivalent phantom for microwaves," *Electron. and Commun. in Japan*, vol. 84, no. 4, 2001.

[18] H.N. Schwerdt *et al.*, "Analysis of electromagnetic fields induced in operation of a wireless fully passive backscattering neurorecording microsystem in emulated human head tissue," *IEEE Trans. Microw. Theory Techn.*, vol. 61, no. 5, pp. 2170–2176, May 2013.
[19] S. Gabriel *et al.*, "The dielectric properties of biological tissues: II. Measurements in the frequency range 10 Hz to 20 GHz," *Phys. Med. Biol.*, vol. 41, pp. 2251–2269, 1996.
[20] Y.-L. Zheng *et al.*, "Unobtrusive sensing and wearable devices for health informatics," *IEEE Trans. Biomed. Eng.*, vol. 61, no. 5, pp. 1538-1554, May 2014.
[21] Z. Wang *et al.*, "Axial ratio enhanced ultra wideband slot spiral on hybrid ebgs," in *Proc. IEEE Int. Symp. Antennas Propagation*, Memphis, TN, July 2014, pp. 1815–1816.
[22] C. Lee *et al.*, "Fully-passive and wireless detection of very-low-power brain signals," in *Proc. Int. Microw. Workshop on RF and Wireless Technol. for Biomed. and Healthcare Appl.*, 2014.
[23] D. Psychoudakis *et al.*, "A portable low-power harmonic radar system and conformal tag for insect tracking," *IEEE Antennas Wireless Propag. Lett.*, vol. 7, 2008.
[24] S.A. Maas, *Microwave Mixers*. Norwood, MA, Artech House, 1993.
[25] Dow Corning, Silastic® MDX4-4210 Biomedical Grade Elastomer. Available: http://www.dowcorning.com
[26] F. Merli *et al.*, "Influence of insulation for implanted antennas," in *Proc. 3rd Europ. Conf. Antennas Propag.*, 2009.
[27] F. Merli *et al.*, "The effect of insulating layers on the performance of implanted antennas," *IEEE Trans. Antennas Propag.*, vol. 59, no. 1, Jan. 2011.
[28] T.A. Szuts *et al.*, "A wireless multi-channel neural amplifier for freely moving animals," *Nature Neurosci.*, vol.14, pp. 263–269, Feb. 2011.
[29] M. Rizk *et al.*, "A single-chip signal processing and telemetry engine for an implantable 96-channel neural data acquisition system," *J. Neural Eng.*, vol. 4, pp. 309–321, 2007.
[30] H. Miranda *et al.*, "HermesD: a high-rate long-range wireless transmission system for simultaneous multichannel neural recording applications," *IEEE Trans. Biomed. Circuits Syst.*, vol. 4, pp. 181–191, Jun. 2010.
[31] M. Yin and M. Ghovanloo, "A low-noise clockless simultaneous 32-channel wireless neural recording system with adjustable resolution," *Analog Integr. Circuits Signal Process.*, vol. 66, pp. 417–431, Nov. 2010.
[32] A.M. Sodagar *et al.*, "A wireless implantable microsystem for multichannel neural recording," *IEEE Trans. Microw. Theory Tech.*, vol. 57, pp. 2565–2573, Oct. 2009.
[33] D.A. Borton *et al.*, "An implantable wireless neural interface for recording cortical circuit dynamics in moving primates," *J. of Neural Eng.*, vol. 10, no.2, Feb. 2013.
[34] M. Rizk *et al.*, "A fully implantable 96-channel neural data acquisition system," *J. Neural Eng.*, vol. 6, Apr. 2009.
[35] A.M. Sodagar *et al.*, "An implantable microsystem for wireless multi-channel cortical recording," in *Proc. IEEE Int. Solid-State Sens. Actuators Microsyst. Conf.*, Lyon, France, 2007.
[36] H.N. Schwerdt *et al.*, "A fully passive wireless backscattering neurorecording microsystem embedded in dispersive human-head phantom medium," *IEEE Electron Div. Lett.*, vol. 33, no. 6, pp. 908–910, Jun. 2012.
[37] J. Kim and Y. Rahmat-Samii, "Implanted antennas inside a human body: Simulations, designs and characterizations," *IEEE Trans. Microw. Theory Tech.*, vol. 52, pp. 1934–1943, Aug. 2005.
[38] *IEEE Standard for Safety Levels With Respect to Human Exposure to Radiofrequency Electromagnetic Fields, 3 kHz to 300 GHz*, IEEE Standard C95.1, 2005.
[39] *Evaluating Compliance with FCC Guidelines for Human Exposure to Radio Frequency Electromagnetic Fields*, FCC OET Bulletin.65, Washington D.C., Aug. 1997.

Asimina Kiourti (S'10–M'14) received the Diploma in electrical and computer engineering from the University of Patras, Patras, Greece, in 2008, the M.Sc. degree in technologies for broadband communications from University College London, London, U.K., in 2009, and the Ph.D. degree in electrical and computer engineering from the National Technical University of Athens, Athens, Greece, in 2013.

She is currently a Senior Research Associate with the ElectroScience Laboratory, The Ohio State University, Columbus, OH, USA. She has authored or coauthored more than 60 journal and conference papers and six book chapters. Her research interests include medical sensing, antennas for medical applications, RF circuits, bioelectromagnetics, and flexible textile and polymer-based antennas.

Dr. Kiourti was the recipient of several awards and scholarships, including the IEEE Engineering in Medicine and Biology Society (EMB-S) Young Investigator Award for 2014, the IEEE Microwave Theory and Techniques Society (MTT-S) Graduate Fellowship for Medical Applications for 2012, and the IEEE Antennas and Propagation Society (AP-S) Doctoral Research Award for 2011.

Cedric W. L. Lee (S'13) received the B.S. (First Class Honors) and M.Sc. degrees in electrical engineering from the National University of Singapore, Singapore, in 2010 and 2013, respectively. He is currently working toward the Ph.D. degree at The Ohio State University, Columbus OH, USA.

He is also a Member of Technical Staff with the DSO National Laboratories, Singapore, where he was involved with the design of antennas prior to his Ph.D. studies. His research interests include RF/microwave circuit and antenna design for radar, wireless communication systems and medical applications.

Mr. Lee was the recipient of the Best Student Paper Award at the IEEE International Microwave Workshop Series on RF and Wireless Technologies for Biomedical and Healthcare Applications in 2014 (IMWS-Bio 2014).

Junseok Chae (SM'11) received the B.S. degree in metallurgical engineering from Korea University, Seoul, Korea, in 1998, and the M.S. and Ph.D. degrees in electrical engineering and computer science from the University of Michigan, Ann Arbor, MI, USA, in 2000 and 2003, respectively.

He joined Arizona State University, Tempe, AZ, USA, in 2005 as an Assistant Professor, and he is currently an Associate Professor of electrical engineering. His areas of interests include microdevices for bioenergy, implantable microdevices, and integrating MEMS with readout/control electronics.

Dr. Chae was the recipient of the First Place prize and the Best Paper Award at the Design Automation Conference Student Design Contest in 2001. He was the recipient of a National Science Foundation CAREER Award on MEMS biosensor array.

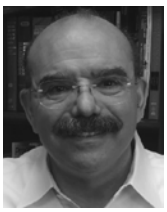

John L. Volakis (S'77–M'82–SM'89–F96) was born in Chios, Greece, on May 13, 1956. He received the B.E. degree (summa cum laude) from Youngstown State University, Youngstown, OH, USA, and the M.Sc. and Ph.D. degrees from The Ohio State

University, Columbus, OH, USA, in 1979 and 1982, respectively.

He started his career at Rockwell International (1982–1984), now Boeing Phantom Works. In 1984, he was appointed an Assistant Professor with the University of Michigan, Ann Arbor, MI, USA, becoming a Full Professor in 1994. He also served as the Director of the Radiation Laboratory from 1998 to 2000. Since January 2003, he has been the Roy and Lois Chope Chair Professor of Engineering at The Ohio State University, Columbus, OH, USA, and also serves as the Director of the ElectroScience Laboratory. He has carried out research on antennas, medical sensing, computational methods, electromagnetic compatibility and interference, propagation, design optimization, RF materials and metamaterials, RFIDs, milli-meter waves and terahertz, body-worn wireless technologies, and multiphysics engineering. His publications include eight books, including Approximate Boundary Conditions in Electromagnetics (IET, 1995), Finite Element Methods for Electromagnetics (Wiley-IEEE Press, 1998) Antenna Engineering Handbook (McGraw-Hill, 2007, 4th ed.), Small Antennas (McGraw-Hill, 2010), and Integral Equation Methods for Electromagnetics (SciTech, 2011)]. His papers include over 350 journal papers, more than 650 conference papers, and 25 book chapters. He has also written several well-edited course packs and has delivered short courses on antennas, numerical methods, and frequency-selective surfaces.

Dr. Volakis is a Fellow of the Applied Computational Electromagnetics Society and a member of the URSI Commissions B and E, and currently serves as the Chair of USNC/URSI Commission B. He was the recipient of the University of Michigan (UM) College of Engineering Research Excellence Award in 1998, and in 2001 he received the UM, Department of Electrical Engineering and Computer Science Service Excellence Award. In 2010 he received the Ohio State University Clara and Peter Scott award for outstanding academic achievement. Also, in 2014 he received the IEEE Antennas and Propagation Society (AP-S) Distiguished Achievement Award and the IEEE AP-S C-T Tai Educator Award. He was listed (2004) by ISI among the top 250 most referenced authors. His mentorship includes over 80 doctoral students/post-doctorals with 30 of them receiving Best Paper awards at international conferences. He was the 2004 President of the IEEE AP-S and served on the AdCom of the IEEE AP-S from 1995 to 1998. He also served as an associate editor for the IEEE TRANSACTIONS ON ANTENNAS AND PROPAGATION from 1988 to 1992, Radio Science from 1994 to 1997, the IEEE Antennas and Propagation Society Magazine (1992–2006), Journal of Electromagnetic Waves and Applications, and URSI Bulletin. Further, he served on the IEEE wide and AP-S Fellows evaluation committee. In 1993 he chaired the IEEE AP-S Symposium and Radio Science Meeting in Ann Arbor, MI, USA, and cochaired the same symposium in 2003 at Columbus, OH, USA.